CONF-9301

ANL/MCT/CP--77181

DE93 006796

OBTAINING HIGH-RESOLUTION IMAGES OF CERAMICS FROM 3-D X-RAY MICROTOMOGRAPHY BY REGION-OF-INTEREST RECONSTRUCTION*

by

E. Anne Sivers, David A. Holloway, and William A. Ellingson

Materials and Components Technology Division

Argonne National Laboratory

Argonne, Illinois 60439-4833

Presented at the 17th Annual Conference on Composites and Advanced Ceramics, Sponsored by the American Ceramic Society, to be held January 10-15, 1993, in Cocoa Beach, Florida.

*Work sponsored by U.S. Department of Energy, Office of Fossil Energy, Advanced Research and Applied Technology, Materials Program.

OBTAINING HIGH-RESOLUTION IMAGES OF CERAMICS FROM 3-D X-RAY MICROTOMOGRAPHY BY REGION-OF-INTEREST RECONSTRUCTION

E. A. Sivers, D. A. Holloway, and W. A. Ellingson

Materials and Components Technology Division
Argonne National Laboratory
Argonne, IL 60439

3-D X-Ray imaging technology, when applied to advanced ceramics, is limited in some cases by detector sensitivity. This limitation can be overcome to some degree by the use of region-of-interest (ROI) reconstruction software. We have developed such software and applied it to 28 mm-diameter, injection-molded Si_3N_4 with known hole-type defects ranging in diameter from 25.4 μm to 508 μm. We have also applied the ROI concept to large (22 cm)-diameter Si_3N_4 turbocharger rotors, demonstrating the ability to resolve only the critical blade-hub region for each blade.

INTRODUCTION

High-resolution, 3-D, x-ray computerized tomographic (XRCT) inspection of large ceramic components often is not practicable because conventional (Global) methods require data that encompasses the entire object. However, it can be useful to inspect small regions of interest (ROI) in large components with high resolution. It is possible to reconstruct data taken from an ROI using unmodified Global methods, but such images suffer from severe "cupping" artifacts that make density determinations impossible and obscure low-contrast features. Specialized variations of Global techniques require additional low-resolution data outside the ROI and long processing times. Local (Lambda)[1,2] ROI XRCT is an alternative that requires no additional data and less processing time than unmodified Global reconstructions. Operationally, Local ROI CT differs from Global only in the convolution filter, but areas of uniform density are "flat", low-contrast detectability is good, and absolute contrast

determination is possible. The primary drawback to Local XRCT is a "ringing" that occurs at the edges of features, but even this characteristic can be an aid in dimensional analysis.

DESCRIPTION OF SYSTEM

The system from which high-resolution ROI images of ceramic components were made is a microfocus (10 μm), 3D XRCT scanner developed by Ellingson and Vannier et al.[3,4] at Argonne National Laboratory. Ceramic components were secured on a turntable between the microfocus x-ray source and an image intensifier in such a way that only an interior cylindrical region of the component was always within the cone of the x-ray source during a 360° rotation. The data was reconstructed using a modified Feldkamp[5] "convolution and backprojection" algorithm. The Global convolution filter is due to Shepp and Logan[6] and the Local convolution filter is due to Faridani et al.[7,8] Local reconstructions are faster because a Local filter is on the order of 5 to 13 samples wide, while a Global filter is as wide as the number of samples in a horizontal row of a 2-D data set. The methods also differ because a small fraction of the simple backprojection of an image is added to its Local reconstruction.

ROI ARTIFACTS, GLOBAL AND LOCAL

In XRCT, an artifact is defined as any difference between the linear attenuation coefficient (scaled CT number) in a reconstructed image and the original object. In this respect, both Global and Local ROI reconstructions have artifacts, but essential information can be extracted from Local reconstructions. Spatial resolution is reproduced faithfully by both, but Local reconstructions exhibit a "ringing" overshoot at the edges of features, the magnitude of which is directly proportional to the contrast difference between the feature and its immediate background. Dimensional analysis is theoretically possible using either method, but the flatness and edge-enhancement of Local reconstructions make automatic processing easier. Contrast between features in a Global reconstruction of ROI data depends strongly upon the part of the object outside of the ROI and "cupping" renders any determination of the actual linear attenuation coefficients in the object inaccurate. The CT numbers inside features in a Local reconstruction of ROI data are proportional to actual linear attenuation coefficients, but also depend upon the size of the features. However, because the magnitude of feature overshoot is directly proportional to the contrast difference between features, it is possible to determine absolute linear attenuation coefficients in Local reconstructions by calibration.

These points are illustrated in Figures 1 - 6, which compare images of Global and Local high-resolution, ROI XRCT reconstructions of Si_3N_4 ceramic phantoms. Figure 1 describes the spatial resolution phantom, a 25 mm-diameter cylinder containing holes of various sizes. A slice of the Global reconstruction shown in Figure 2 illustrates the cupping artifact that masks the 25.4 μm hole. The same slice of the Local reconstruction in Figure 3 shows all of the holes clearly. Figure 4 describes the contrast detectability phantom, a 28.5 mm-diameter cylinder of Si_3N_4 injection molding mix containing 15.5% organic binder by weight. Embedded in the cylinder are five plugs of the mix containing percentages of organic binder that vary from 2 % to 14.5 %. The Global reconstruction in Figure 5 is so cupped that the plugs appear to have nonuniform density. The Local reconstruction in Figure 6 shows that the density of each plug is uniform and that all are different.

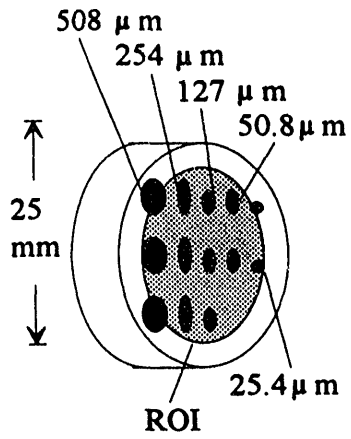

Figure 1 Ceramic resolution phantom

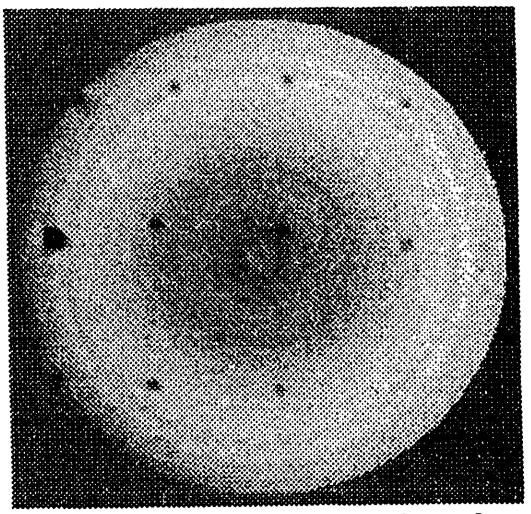

Figure 2 Global reconstruction of resolution phantom

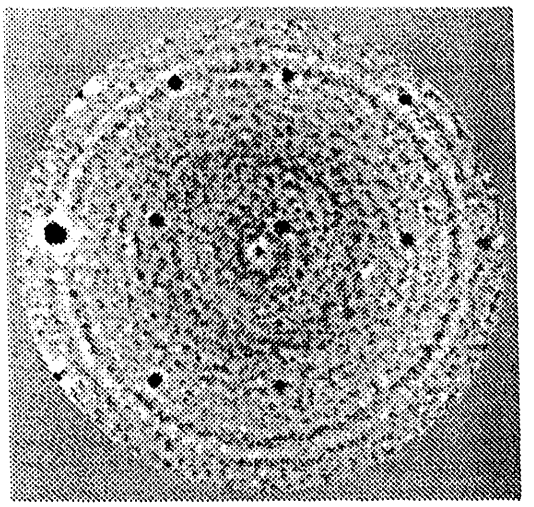

Figure 3 Local reconstruction of resolution phantom

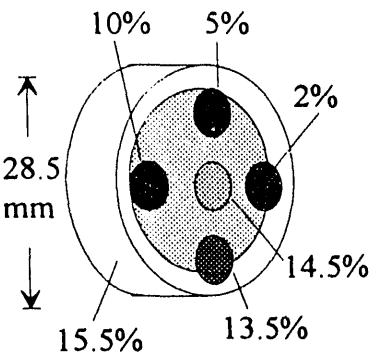

Figure 4 Ceramic density phantom

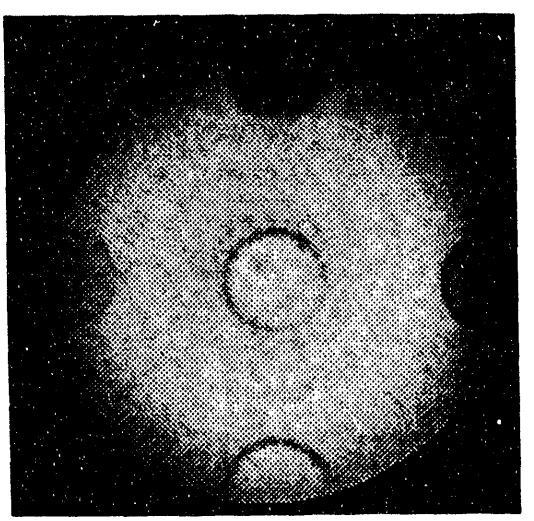

Figure 5 Global reconstruction of density phantom

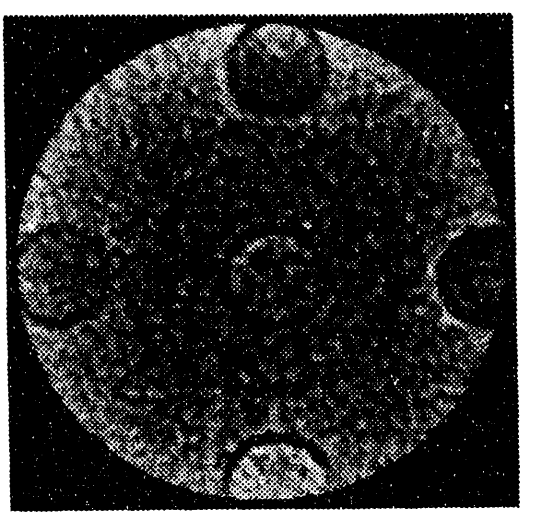

Figure 6 Local reconstruction of density phantom

CONTRAST IN LOCAL CT

Because the determination of absolute contrast in Local XRCT is somewhat complicated, computer simulations are used to illustrated the method. It is the peak-to-peak fluctuation at the edges of features in a Local reconstruction that is actually proportional to their contrast, rather than the CT number measured inside them. Figure 7 describes a simulated cylinder with embedded features of different sizes having 100% contrast (twice the linear attenuation coefficient of the cylinder). Figure 8 shows one slice of a Local reconstruction of this cylinder. Figure 9 is a graph of the contrast in the center of each feature plotted as a function of the diameter of the feature (normalized by the width of the convolution filter). This plot implies that the overshoot at edges raises the contrast measured inside small features, but that it has little effect on the Local contrast in the center of large features. It is true that measured contrast inside a feature increases linearly with true contrast, but the value will depend upon the feature size. This conclusion is supported by the simulation of a cylinder with embedded features all which have a diameter 8.5 times the width of the convolution filter, but different contrast. A sketch of the phantom is shown in Figure 10 and the Local reconstruction, in Figure 11. Figure 12 is a graph of measured contrast plotted as a function of actual contrast.

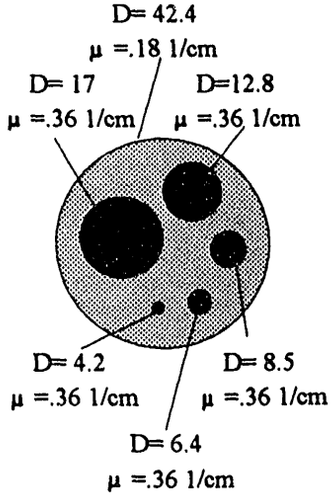

Figure 7 Simulated size/contrast phantom

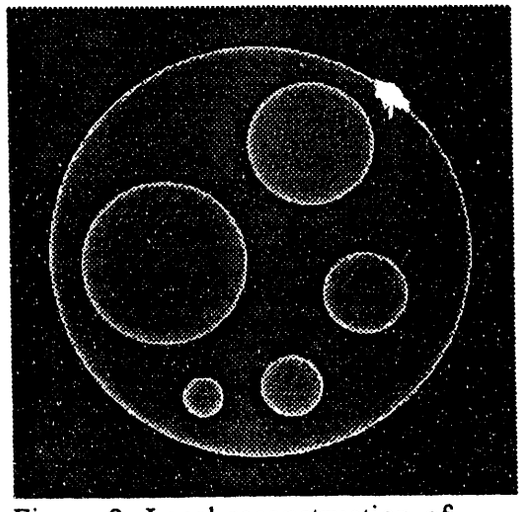

Figure 8 Local reconstruction of size/contrast phantom

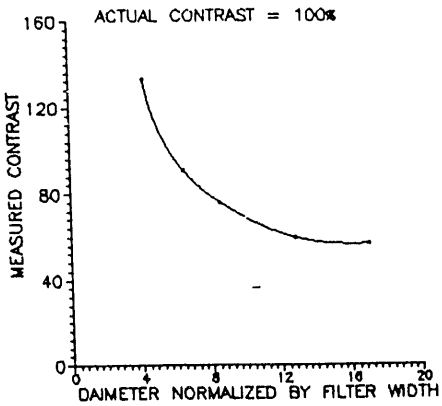

Figure 9 Graph of contrast vs feature diameter

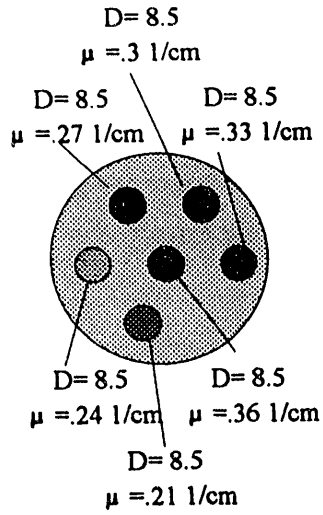

Figure 10 Simulated contrast phantom

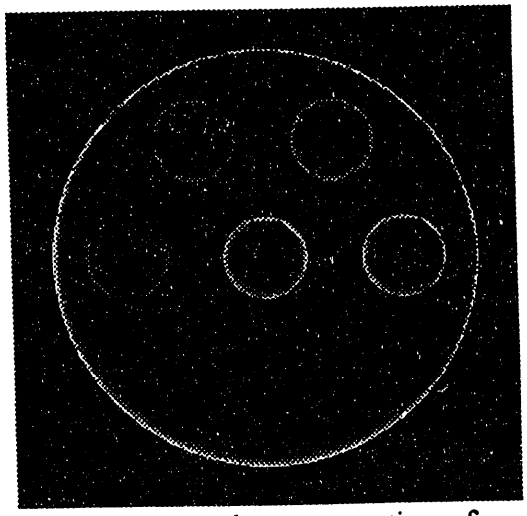

Figure 11 Local reconstruction of contrast phantom

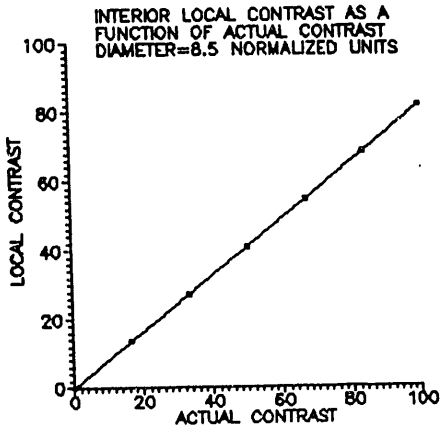

Figure 12 Measured contrast plotted as a function of actual contrast

Fortunately, it is possible to determine the contrast in Local CT regardless of feature size by measuring the peak-to-peak variation of the overshoot at the edges of features. Figure 13 is a graph of the peak-to-peak variation of the overshoot as a function of feature size and actual contrast for the five different diameters shown in Figure 7. Although this measurement is somewhat sensitive to statistical noise, relative contrast can be measured, and absolute contrast can be computed if a calibration can be performed.

NOISE IN LOCAL CT

The smallest contrast difference that can be detected in a reconstruction is limited by statistical noise on the image. It is difficult to compare the amount of noise on Global and Local ROI reconstructions because their relative scaling is somewhat arbitrary. One measure of noise amplification is the sum of the squares of the convolution filter terms. The sum of the squares of the Local filter terms is about 1.3 times larger than that of the Shepp-Logan Global filter. This means that, other factors being equal, the standard deviation of the reconstruction noise on the Local reconstruction is about 1.13 times larger. However, because of cupping on Global ROI reconstructions and non-linear mapping of Local reconstructions, they are seldom scaled identically. Figure 14 is a superposition of line plots of row 109 (out of 255) from the Global and Local reconstructions of the hole phantom shown in Figures 2 and 3. The reconstructions are scaled such that the true contrast in the 508 μm hole is the same for both and the noise is seen to be comparable.

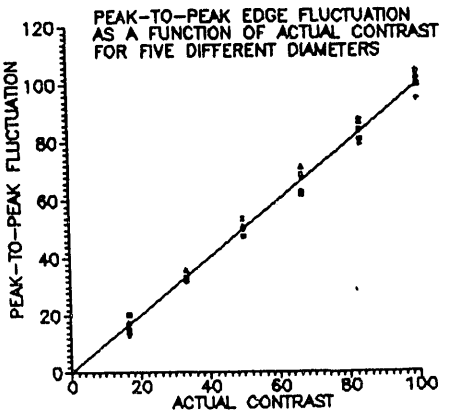

Figure 13 Peak-to-peak fluctuation vs actual contrast (5 diameters).

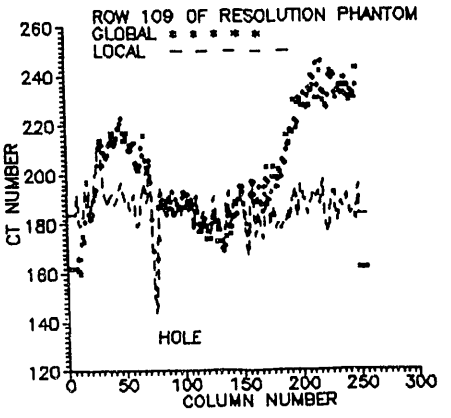

Figure 14 Line profiles of row 109 from Figs. 2 and 3

Often, noise on a Local reconstruction appears to be higher than noise on a comparable Global reconstruction because a larger scaling factor is needed to encompass cupping on the latter. Figure 15 illustrates the ROI taken near one edge of a large Si_3N_4 turbine rotor. The Global reconstruction in Figure 16 appears to be less noisy than the Local reconstruction Figure 17, but this is due to the difference in scaling factors. Figure 18 shows a superposition of columns 143 (out of 255) from the Global and Local reconstructions that reveals the cupping of the Global reconstruction and the compressed scale of the Local reconstruction. In fact, it is possible to obtain much better statistics in an ROI data set because, without the need for air readings, the x-ray detector must accommodate a much narrower range of flux. It is even possible to tailor the x-ray output such that higher flux is used to penetrate thicker parts of an irregularly shaped component.

CONCLUSION

It has been demonstrated that ROI, 3-D XRCT has great potential for inspecting small regions of large ceramic components with high resolution. Local CT methods make possible dimensional analysis and density determinations without taking data outside the selected region and without long processing times.

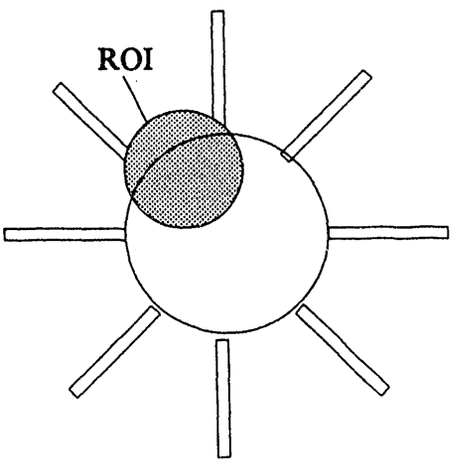

Figure 15 Simplified sketch of ceramic turbine rotor

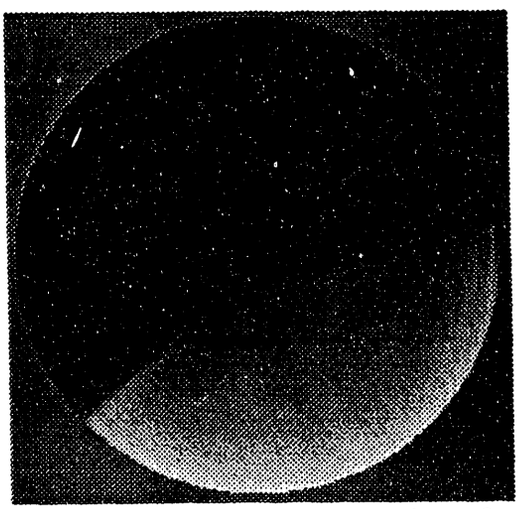

Figure 16 Global reconstruction of turbine rotor ROI

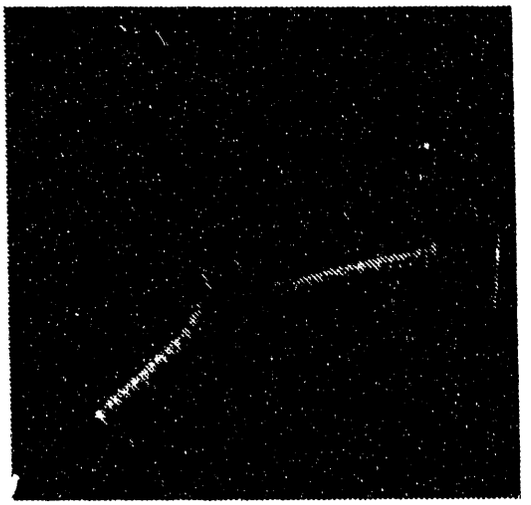

Figure 17 Local reconstruction of turbine rotor ROI

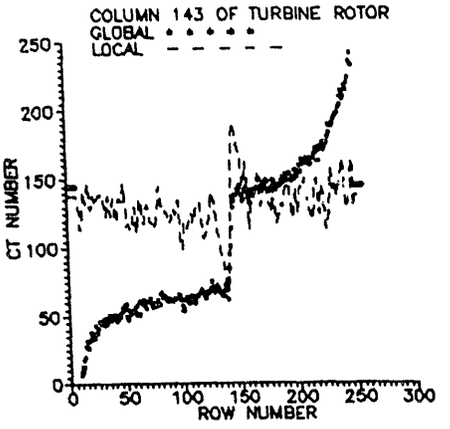

Figure 18 Line profiles of column 143 from Figs. 16 and 17

ACKNOWLEDGMENTS

This work was sponsored by the U.S. Department of Energy, Office of Fossil Energy, Advanced Research and Applied Technology, Materials Program. The authors would like to thank Kennan Smith and Adel Faridani of the University of Oregon, Corvallis, for invaluable discussions and recommendations.

REFERENCES

1. E. I. Vainberg, I. A. Kazak, and M. L. Faingoiz, "Reconstruction of the Internal Three-Dimensional Structure of Objects Based on Real-Time Integral Projections," *Soviet J. Nondest. Test.*, Vol. 17, pp. 415-423, (1981).

2. K. T. Smith, and F. Keinert, "Mathematical Foundations of Computed Tomography," *Appl. Optics*, Vol. 24, No. 23, pp. 3950-3957, (1985).

3. W. A. Ellingson and M. W. Vannier, "X-Ray Computed Tomography for Nondestructive Evaluation of Advanced Structural Ceramics," Argonne National Laboratory Report ANL -87-52, (1989).

4. W. A. Ellingson, M. W. Vannier, and D. P. Stintor, "Application of X-Ray Computed Tomography to Ceramic/Ceramic Composites," pp. 9-25, Characterization of Advanced Materials, W. Altergath and E. Henneke, eds., Plenum Press, New York, (1991).

5. L. Feldkamp, L. Davis, and J. Kress, "Practical Cone-Beam Algorithm," *J. Opt. Soc. Am. A*, Vol. 1, No. 6, pp. 612-622, (1984).

6. L. A. Shepp, and B. F. Logan, "The Fourier Reconstruction of a Head Section", *IEEE Trans. Nuc. Sci.*, Vol NS21, pp. 21-43, (1974).

7. A. Faridani, F. Keinert, F. Natterer, E. L. Ritman, and K. T. Smith, "Local and Global Tomography," pp. 241-255, Signal Processing, Part II, Control Theory and its Application, F. A. Grunbaum, ed., Springer Verlag, New York, (1990).

8. A. Faridani, E. L. Ritman, and K. T. Smith, "Local Tomography," *SIAM J. Appl. Math.*, Vol. 52, No. 2, pp. 459-484, (1992)

END

DATE
FILMED
2/19/93